Loss of natriuretic peptide receptor C enhances sinoatrial node dysfunction in aging and frail mice

Supplementary Material

Supplemental Methods

Mouse clinical frailty assessment

Frailty was assessed in mice using the mouse clinical FI. Assessments of the integument, musculoskeletal, vestibulocochlear/auditory, ocular, nasal, digestive, urogenital and respiratory systems were performed. Signs of discomfort, body temperature and body mass were also assessed. Each item was given a score of 0 (no sign of deficit), 0.5 (mild deficit) or 1 (severe deficit). Deficits in body temperature and body mass were scored based on deviation from the mean in all mice. The scores for each item were added together and the sum was divided by the number of items measured (i.e. 31 items) to yield an FI score between 0 and 1.

In vivo electrophysiology

HR was measured in anesthetized mice (2% isoflurane inhalation) using 30-gauge subdermal needle electrodes (Grass Technologies) to record body surface (lead II) ECGs. In parallel, a 1.2 French octapolar electrophysiology catheter was inserted in the right heart via the jugular vein and used for intracardiac programmed stimulation experiments. All stimulation pulses were given at 3 V for 2 ms, which enabled continuous capture and drive of cardiac conduction. Sinoatrial node recovery time (SNRT) was measured by delivering a 12-stimulus drive train at a cycle length of 100 ms. SNRT is defined as the time between the last stimulus in the drive train and the occurrence of the first spontaneous atrial beat (P wave). SNRT was

corrected for heart rate (cSNRT) by subtracting the prestimulus RR interval from the measured SNRT. Data were acquired using a Gould ACQ-7700 amplifier and Ponemah Physiology Platform software (Data Sciences International). Body temperature was monitored continuously via a rectal probe and maintained at 37°C with a heating pad.

High-resolution optical mapping

To investigate patterns of electrical conduction in the SAN we used high resolution optical mapping in atrial preparations. Hearts were excised into Krebs solution (37°C) containing (in mM): 118 NaCl, 4.7 KCl, 1.2 KH_2PO_4, 25 $NaHCO_3$, 1 $CaCl_2$, 1 $MgCl_2$, 11 glucose and bubbled with 95% O_2/5% CO_2 to maintain a pH of 7.4. The atrial preparation was superfused continuously with Krebs solution (37°C) bubbled with 95% O_2/5% CO_2 and allowed to equilibrate for at least 10 min. The preparation was then incubated with the voltage-sensitive dye RH-237 (15 μM; Biotium) for 15 min. After the dye incubation period, superfusion was resumed with blebbistatin (10 μM; Cayman Chemical Company) added to the superfusate to suppress contractile activity and prevent motion artifacts. Experiments were performed in sinus rhythm so that the cycle length (i.e. beating rate) of the atrial preparation was free to change. RH-237-loaded atrial preparations were illuminated with light from the X-Cite Xylis Broad Spectrum LED Illumination System (Excelitas Technologies) and filtered with a 520/35 nm excitation filter (Semrock). Emitted fluorescence was separated by a dichroic mirror (560 nm cut-off; Semrock) and filtered by a 715 nm long-pass emissions filter (Andover Corp.). Recordings were captured using a high-speed CMOS camera (MiCAM03-N256, SciMedia). We mapped conduction in the region of the right atrial posterior wall around the point of initial electrical excitation, which corresponds to the activation of the SAN. The region that was mapped

extended from the superior vena cava to the inferior cava along the edge of the crista terminalis, based on the known anatomical location of the SAN in the mouse heart. Data were captured from an optical field of view of 6.8 x 6.8 mm at a frame rate of 1000 or 3000 frames/s using BrainVision software (BrainVision Inc.). The spatial resolution was 26.6 x 26.6 μM for each pixel. Magnification was constant in all experiments and no pixel binning was used. All optical data were analyzed using custom software written in MATLAB® (Mathworks) as we have previously described.

Quantitative PCR

Quantitative gene expression was performed in isolated SAN tissue. Intron spanning primers for *npr3* (NPR-C), *cacna1c* ($Ca_V1.2$), *cacna1d* ($Ca_V1.3$), *hcn1* (HCN1), *hcn2* (HCN2), *hcn4* (HCN4), *col1a* (collagen type I), *col3a* (collagen type III), *tgfb1* (transforming growth factor β), *mmp9* (matrix metalloproteinase 9), as well as *timp1*, *timp2*, *timp3* and *timp4* (tissue inhibitor of metalloproteinase 1-4) were used. *gapdh* (GAPDH) was used as a reference gene in all experiments except for *npr3* expression studies which used *hprt1* (hypoxanthine phosphoribosyltransferase 1) as a reference gene. Primer sequences are provided Supplemental Table 1. Following synthesis, primers were reconstituted in nuclease free water at a concentration of 100 μM and stored at -20°C. All primer sets were validated in order to determine optimal annealing temperature as well as confirmation of ideal amplification efficiency (between 90-110% copy efficiency per cycle). RNA was extracted in PureZOL™ RNA isolation reagent according to kit instructions (Aurum Total RNA Fatty and Fibrous Tissue Kit, Bio-Rad). RNA was eluted in 40 μl of elution buffer from the spin column. RNA purity and quantity were determined using a NanoPhotometer (Implen). First strand synthesis reactions

were performed using the iScript cDNA synthesis kit (Bio-Rad) according to kit instructions. Lack of genomic DNA contamination was verified by reverse transcription (RT)-PCR using a no RT control. RT-qPCR using BRYT green dye (Promega) was used to assess gene expression.

Collagen staining and immunohistochemistry

Fibrosis in the SAN was assessed using picrosirius red staining on paraffin embedded sections (5 μm) through the SAN. The myocardium was counterstained using fast green. The SAN region was confirmed using HCN4 immunostaining in adjacent sections. The level of fibrosis was quantified using ImageJ software.

Plasma creatinine

Plasma creatinine was measured using a creatinine assay kit (Abcam) according to the manufacturer's instructions.

Echocardiography

Cardiac structure was assessed by echocardiography in mice anesthetized y isoflurane inhalation (2%) using a Vevo 3100 ultrasound machine (Fujifilm VisualSonics).

Supplemental Figures

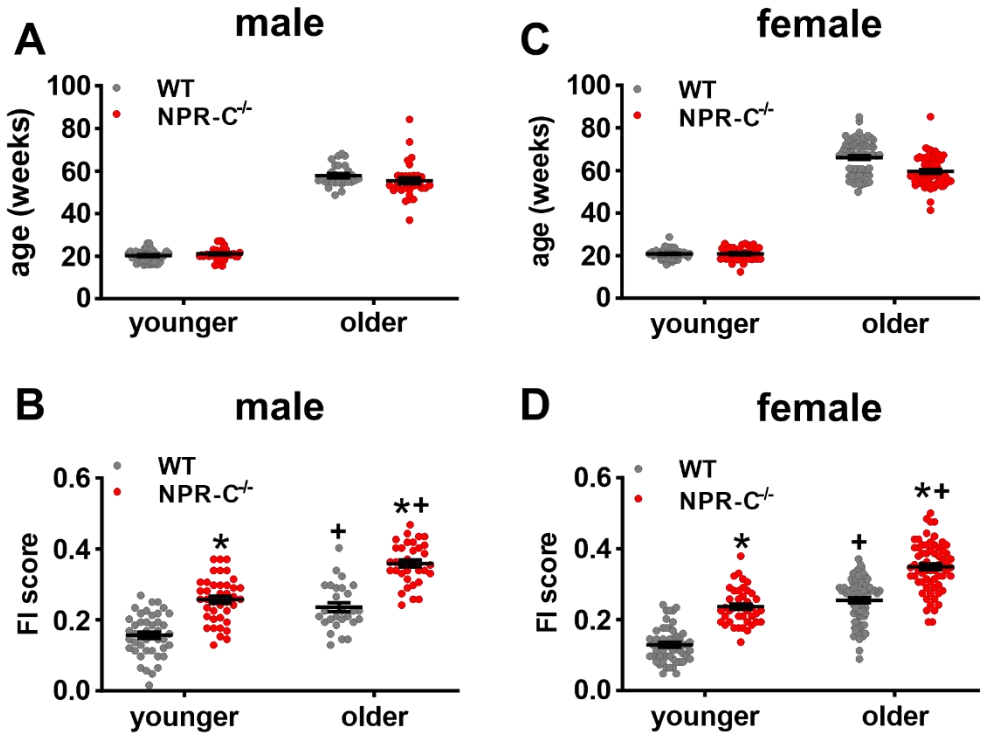

Supplemental Figure 1. Ages and frailty index scores for male and female WT and NPR-C$^{-/-}$ mice. (**A**) Ages of male younger and older WT and NPR-C$^{-/-}$ mice used in this study; *n*=44 mice for WT-younger, 27 for WT-older, 40 for NPR-C$^{-/-}$-younger and 34 for NPR-C$^{-/-}$-older. (**B**) Frailty index (FI) scores in male younger and older WT and NPR-C$^{-/-}$ mice used in this study (same mice as panel **A**). (**C**) Ages of female younger and older WT and NPR-C$^{-/-}$ mice used in this study; *n*=53 mice for WT-younger, 77 for WT-older, 42 for NPR-C$^{-/-}$-younger and 66 for NPR-C$^{-/-}$-older. (**D**) FI scores in female younger and older WT and NPR-C$^{-/-}$ mice used in this study (same mice as panel **C**). *P<0.05 vs. WT, ^{+}P<0.05 vs. younger by two-way ANOVA with a Tukey posthoc test.

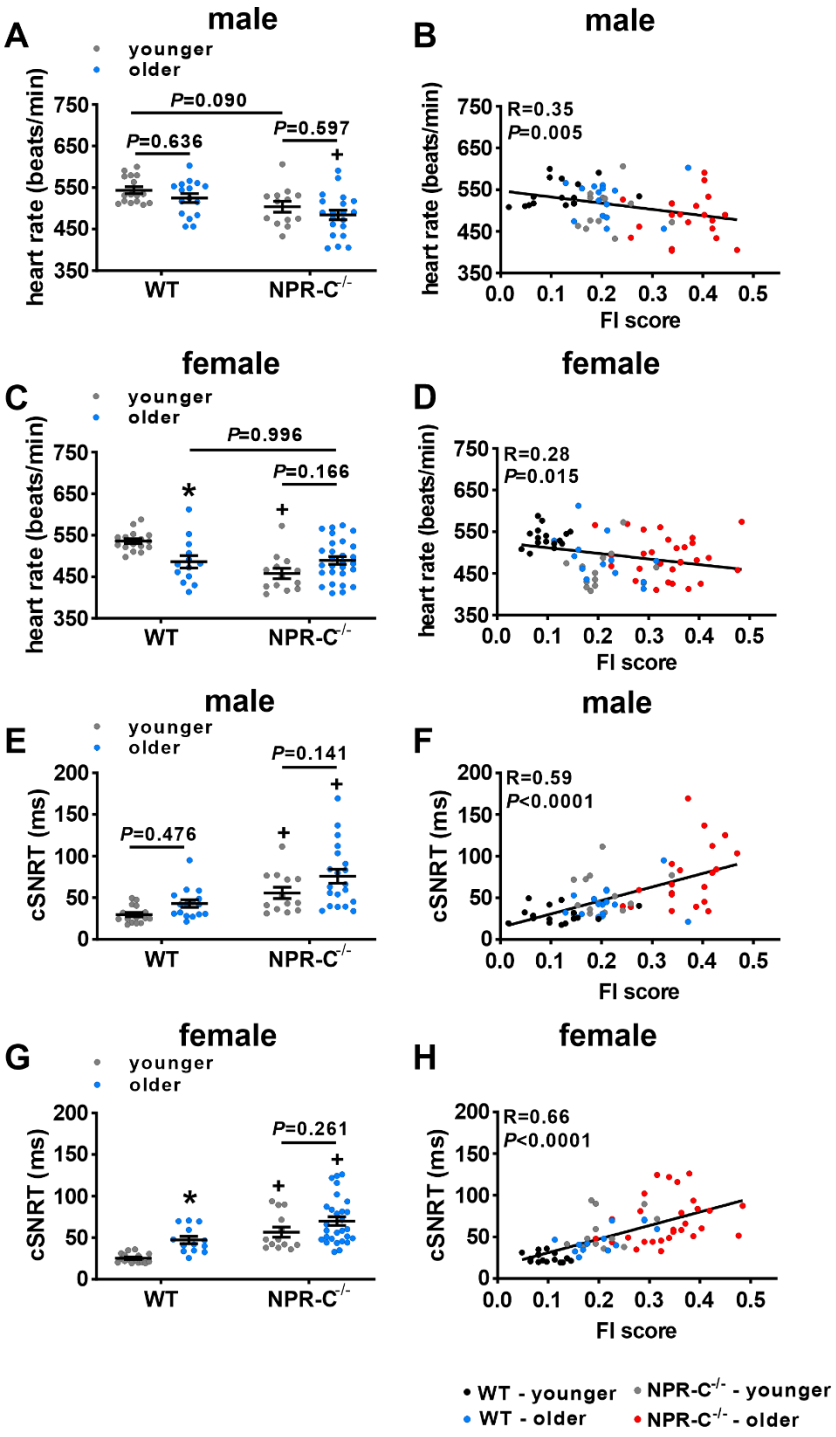

Supplemental Figure 2. Heart rate and corrected sinoatrial node recovery time in male and female WT and NPR-C$^{-/-}$ mice. (**A**) Heart rate in male younger and older WT and NPR-C$^{-/-}$ mice. (**B**) Heart rate in male younger and older WT and NPR-C$^{-/-}$ mice as function of FI score (same mice as panel **A**). (**C**) Heart rate in female younger and older WT and NPR-C$^{-/-}$ mice. (**D**) Heart rate in female younger and older WT and NPR-C$^{-/-}$ mice as a function of FI score (same mice as panel **C**). (**E**) Corrected sinoatrial node recovery time (cSNRT) in male younger and older WT

and NPR-C$^{-/-}$ mice. (**F**) cSNRT in male younger and older WT and NPR-C$^{-/-}$ mice as function of FI score (same mice as panel **E**). (**G**) cSNRT in female younger and older WT and NPR-C$^{-/-}$ mice. (**H**) cSNRT in female younger and older WT and NPR-C$^{-/-}$ mice as function of FI score (same mice as panel **G**). For panels **A**, **C**, **E,** and **G** *P<0.05 vs. younger, ^{+}P<0.05 vs. WT by two-way ANOVA with a Tukey posthoc test. For panels **B**, **D**, **F,** and **H** linear regressions analyzed using Pearson's correlation. For male mice n=16 mice for WT-younger, 16 for WT-older, 13 for NPR-C$^{-/-}$-younger and 20 for NPR-C$^{-/-}$-older. For female mice n=16 mice for WT-younger, 13 for WT-older, 13 for NPR-C$^{-/-}$-younger and 28 for NPR-C$^{-/-}$-older.

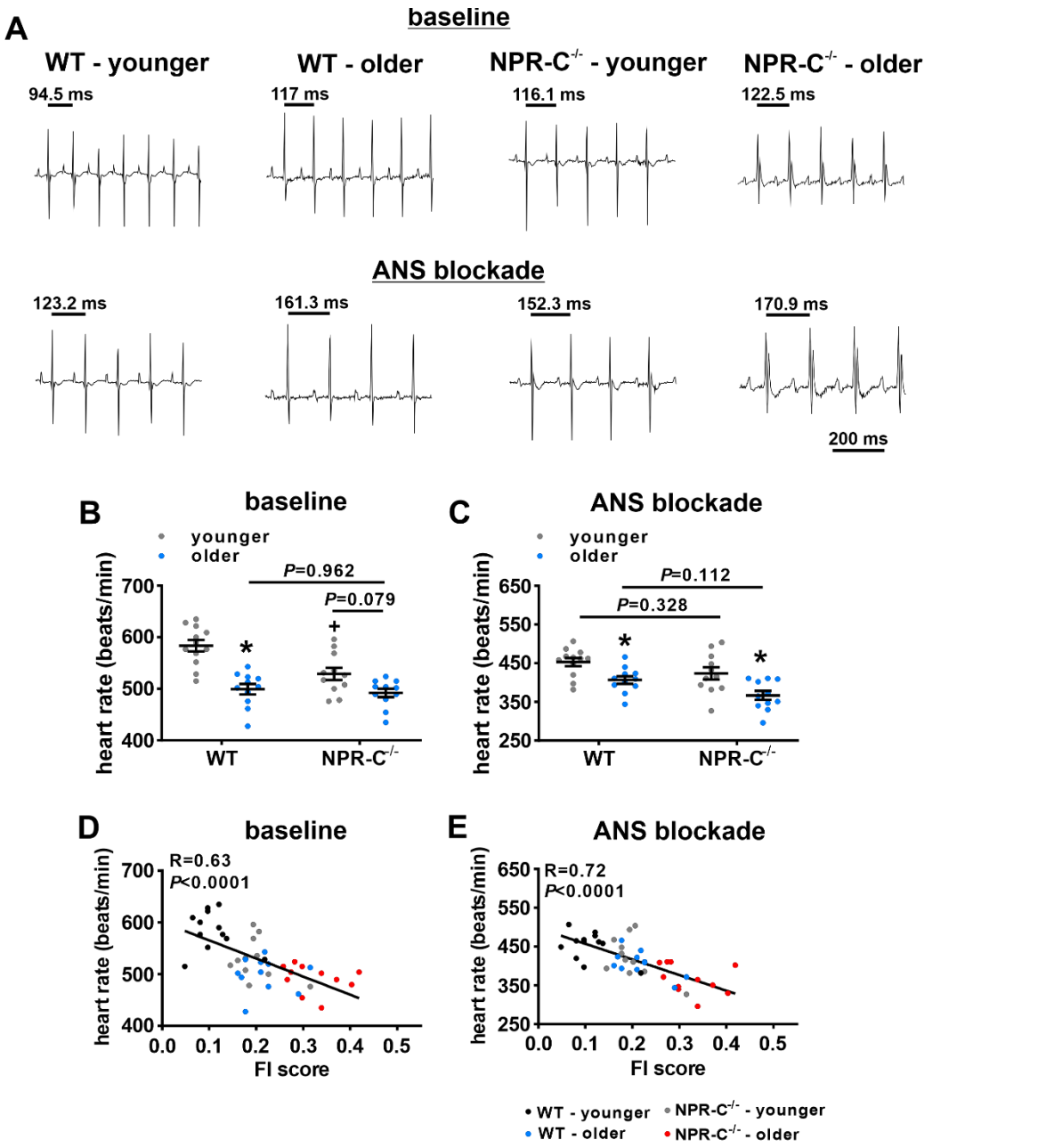

Supplemental Figure 3. Effects of age and frailty on intrinsic heart rate measured during autonomic nervous system blockade in WT and NPR-C$^{-/-}$ mice. Autonomic nervous system (ANS) blockade was achieved by intraperitoneal injection of atropine (10 mg/kg) and propranolol (10 mg/kg). (**A**) Representative ECGs in younger and older WT and NPR-C$^{-/-}$ mice at baseline and after ANS blockade. (**B** and **C**) Heart rate at baseline (**B**) and after ANS blockade (**C**) in younger and older WT and NPR-C$^{-/-}$ mice. *P<0.05 vs. younger, ^{+}P<0.05 vs. WT by two-way ANOVA with a Tukey posthoc test; n=12 mice for WT-younger, 11 for WT-older, 11 for NPR-C$^{-/-}$-younger and 11 for NPR-C$^{-/-}$-older. (**D** and **E**) Heart rate at baseline (**D**) and after ANS blockade (**E**) in younger and older WT and NPR-C$^{-/-}$ mice as function of FI score (same mice as panels **B** and **C**). Linear regressions analyzed using Pearson's correlation.

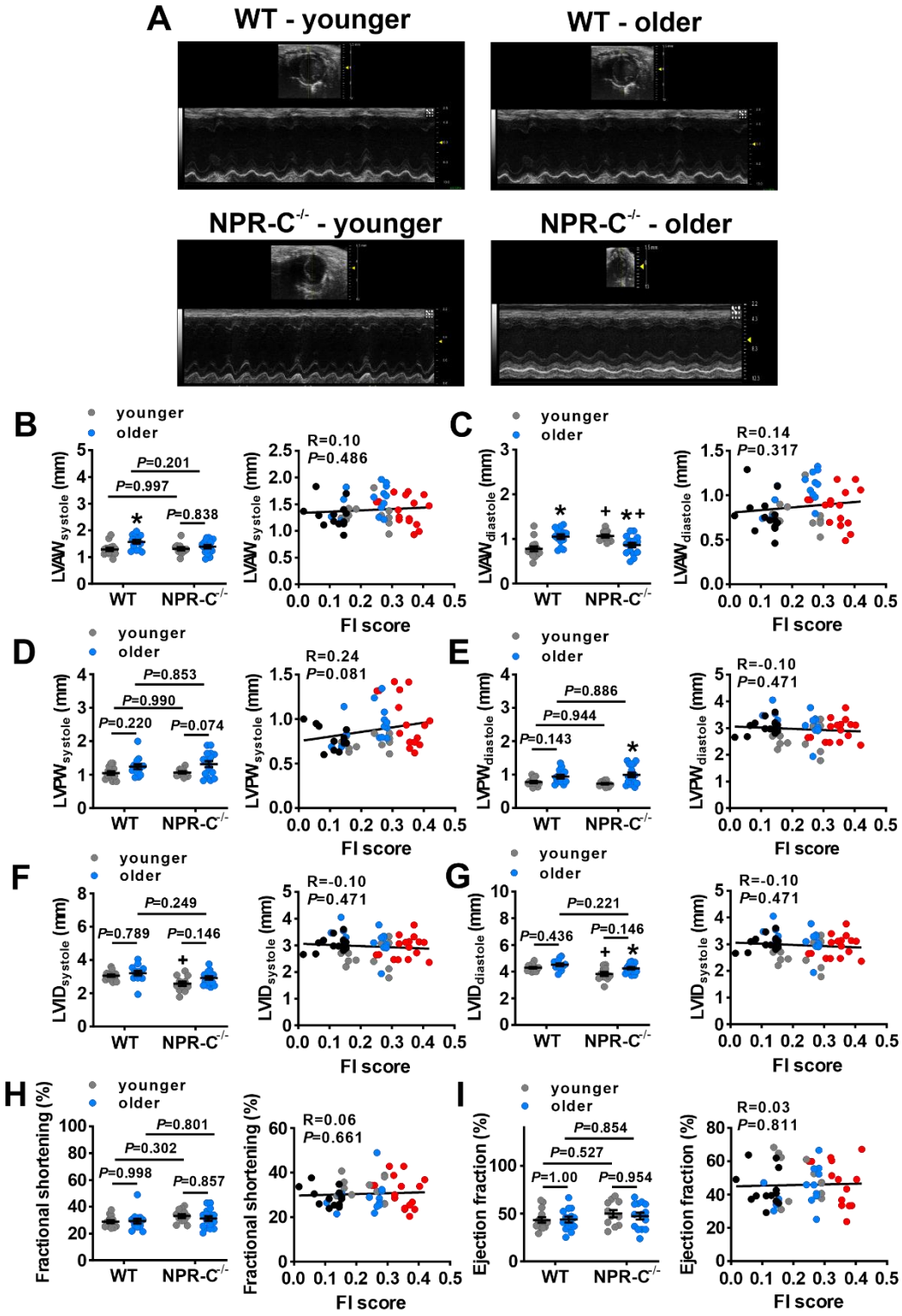

Supplemental Figure 4. Echocardiography in WT and NPR-C$^{-/-}$ mice. (**A**) Representative M-mode images measured from the short axis in younger and older WT and NPR-C$^{-/-}$ mice. (**B-C**) left ventricular anterior wall (LVAW) thickness in systole (**B**) and diastole (**C**) as a function of

age/genotype (left) and FI score (right). (**D-E**) left ventricular posterior wall (LVPW) thickness in systole (**D**) and diastole (**E**) as a function of age/genotype (left) and FI score (right). (**F-G**) left ventricular internal diameter (LVID) in systole (**F**) and diastole (**G**) as a function of age/genotype (left) and FI score (right). (**H-I**) ejection fraction (**H**) and fractional shortening (**I**) as a function of age/genoptye (left) and FI score (right). **P*<0.05 vs. younger, ^{+}P<0.05 vs. WT by two-way ANOVA with a Tukey posthoc test. Linear regressions analyzed using Pearson's correlation. *n*=14 mice for WT-younger, 14 for WT-older, 11 for NPR-$C^{-/-}$-younger and 16 for NPR-$C^{-/-}$-older.

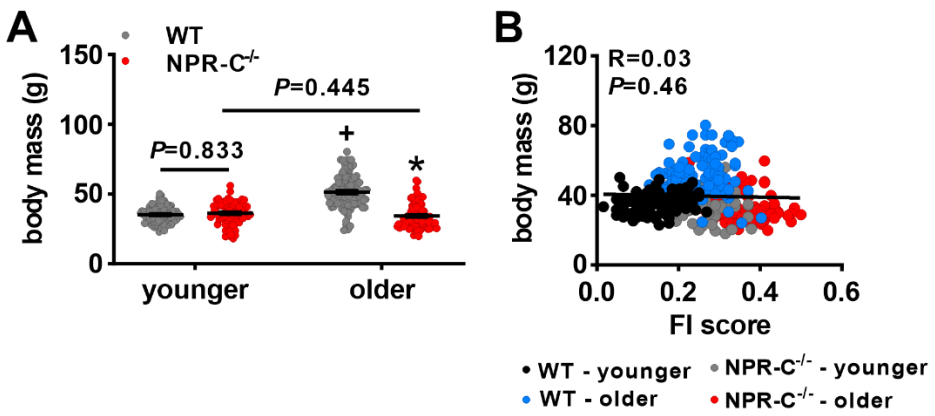

Supplemental Figure 5. Body mass in wildtype and NPR-C$^{-/-}$ mice. (**A**) Body mass in younger and older WT and NPR-C$^{-/-}$ mice used in this study; *n*=97 mice for WT-younger, 103 for WT-older, 82 for NPR-C$^{-/-}$-younger and 100 for NPR-C$^{-/-}$-older; **P*<0.05 vs. WT, $^{+}$*P*<0.05 vs. younger by two-way ANOVA with a Tukey posthoc test. (**B**) Body mass a function of FI score (same mice as panel A). Linear regression analyzed using Pearson's correlation.

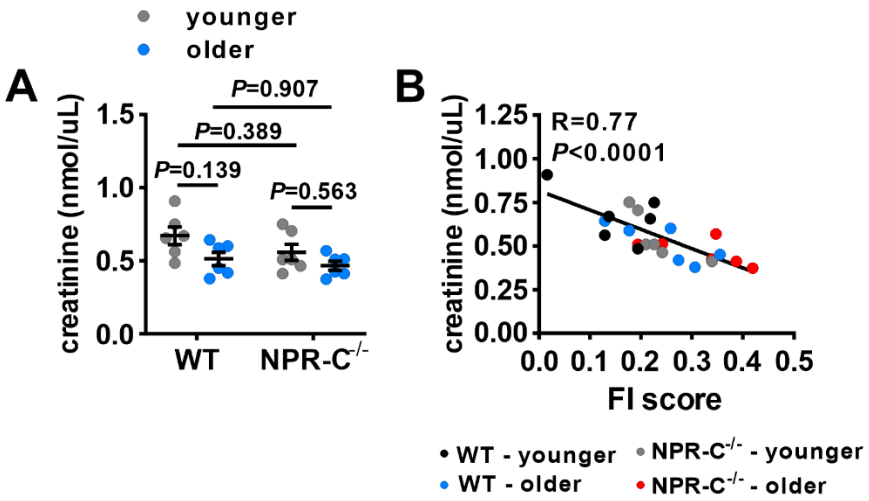

Supplemental Figure 6. Effects of age and frailty on plasma creatinine in WT and NPR-C$^{-/-}$ mice. (**A**) serum creatinine in younger and older WT and NPR-C$^{-/-}$ mice. *P<0.05 vs. younger, ^{+}P<0.05 vs. WT by two-way ANOVA with a Tukey posthoc test. (**B**) serum creatine as a function of FI score for younger and older WT and NPR-C$^{-/-}$ mice (same mice as panel A). Linear regression analyzed using Pearson's correlation. n=6 mice for WT-younger, 6 for WT-older, 6 for NPR-C$^{-/-}$-younger and 6 for NPR-C$^{-/-}$-older.

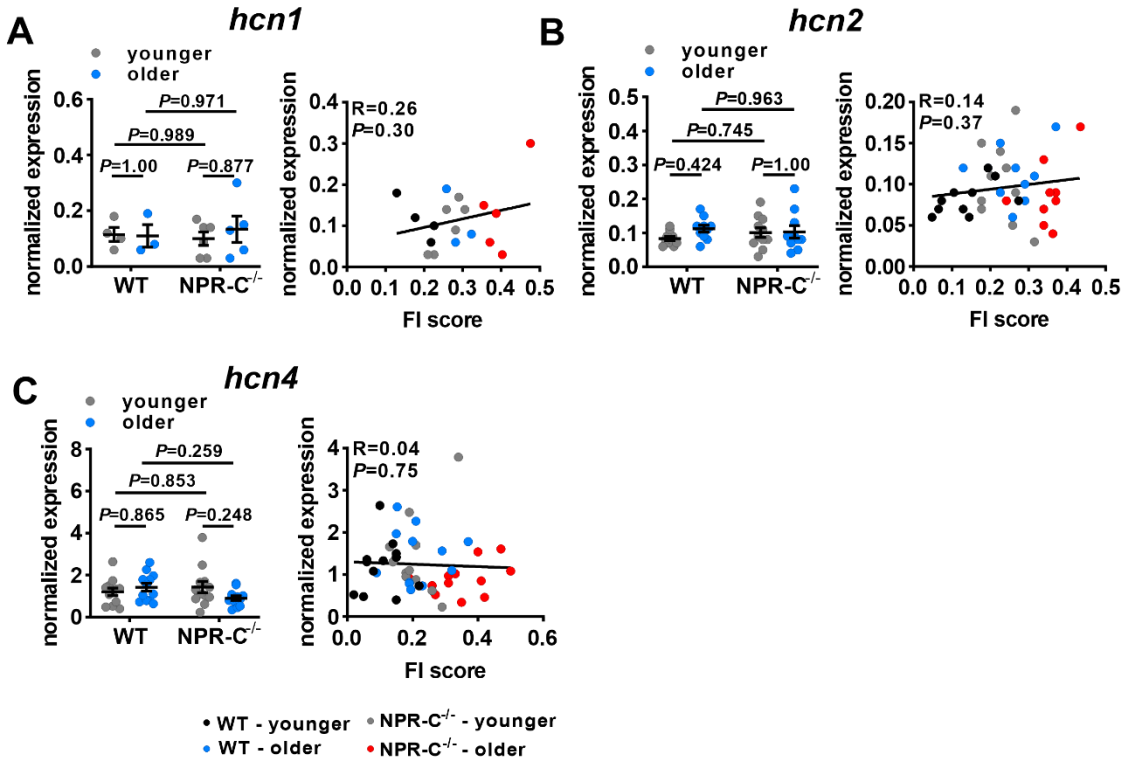

Supplemental Figure 7. Effects of age and frailty on sinoatrial node HCN mRNA expression in WT and NPR-C$^{-/-}$ mice. (**A**) mRNA expression of *hcn1* in younger and older WT and NPR-C$^{-/-}$ mice (left panel) and as a function of FI score (right panel); *n*=4 mice for WT-younger, 3 for WT-older, 6 for NPR-C$^{-/-}$-younger and 5 for NPR-C$^{-/-}$-older. (**B**) mRNA expression of *hcn2* in younger and older WT and NPR-C$^{-/-}$ mice (left panel) and as a function of FI score (right panel); *n*=10 mice for WT-younger, 10 for WT-older, 11 for NPR-C$^{-/-}$-younger and 10 for NPR-C$^{-/-}$-older. (**C**) mRNA expression of *hcn4* in younger and older WT and NPR-C$^{-/-}$ mice (left panel) and as a function of FI score (right panel); *n*=12 mice for WT-younger, 12 for WT-older, 12 for NPR-C$^{-/-}$-younger and 12 for NPR-C$^{-/-}$-older. For figures as a function of chronological age and genotype **P*<0.05 vs. younger; $^{+}$*P*<0.05 vs. WT by two-way ANOVA with a Tukey posthoc test. For figures as a function of FI score linear regressions analyzed using Pearson's correlation.

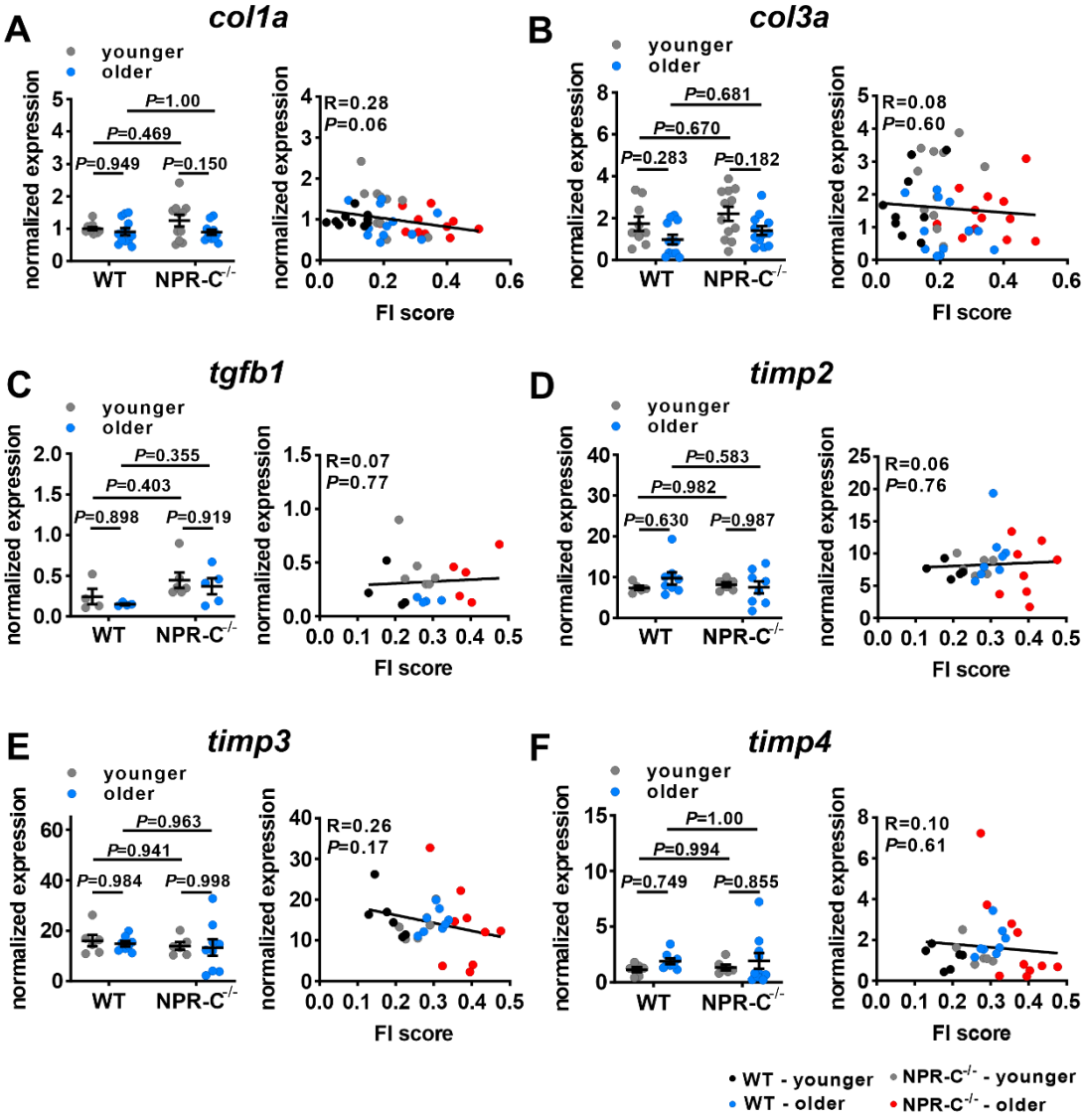

Supplemental Figure 8. Effects of age and frailty on mRNA expression of profibrotic genes in the sinoatrial node in WT and NPR-C$^{-/-}$ mice. (**A**) mRNA expression of *col1a* in younger and older WT and NPR-C$^{-/-}$ mice (left panel) and as a function of FI score (right panel); *n*=10 mice for WT-younger, 12 for WT-older, 11 for NPR-C$^{-/-}$-younger and 11 for NPR-C$^{-/-}$-older. (**B**) mRNA expression of *col3a* in younger and older WT and NPR-C$^{-/-}$ mice (left panel) and as a function of FI score (right panel); *n*=9 mice for WT-younger, 12 for WT-older, 12 for NPR-C$^{-/-}$-younger and 12 for NPR-C$^{-/-}$-older. (**C**) mRNA expression of *tgfb1* in younger and older WT and NPR-C$^{-/-}$ mice (left panel) and as a function of FI score (right panel); *n*=4 mice for WT-younger, 4 for WT-older, 6 for NPR-C$^{-/-}$-younger and 5 for NPR-C$^{-/-}$-older. (**D**) mRNA expression of *timp2* in younger and older WT and NPR-C$^{-/-}$ mice (left panel) and as a function of FI score (right panel); *n*=5 mice for WT-younger, 8 for WT-older, 6 for NPR-C$^{-/-}$-younger and 8 for NPR-C$^{-/-}$-older. (**E**) mRNA expression of *timp3* in younger and older WT and NPR-C$^{-/-}$ mice (left panel) and as a function of FI score (right panel); *n*=6 mice for WT-younger, 8 for WT-older, 6 for NPR-C$^{-/-}$-younger and 9 for NPR-C$^{-/-}$-older. (**F**) mRNA expression of *timp4* in younger and older WT and NPR-C$^{-/-}$ mice (left panel) and as a function of FI score (right panel); *n*=6 mice for

WT-younger, 8 for WT-older, 6 for NPR-C$^{-/-}$-younger and 10 for NPR-C$^{-/-}$-older. For figures as a function of chronological age and genotype *P<0.05 vs. younger; ^{+}P<0.05 vs. WT by two-way ANOVA with a Tukey posthoc test. For figures as a function of FI score linear regressions analyzed using Pearson's correlation.

Supplemental Table 1: Quantitative PCR primers

Gene of Interest	Forward Primer (5' → 3')	Reverse Primer (3' → 5')	Amplicon Length
Npr3	CGAGCGAGTGGTGATCATGTGTG	CTCCACGAGCCATCTCCGTAGG	147
Cacna1c	ATGATTCGGGCCTTTGTTCAG	TGGAGTAGGGATGTGCTCG	228
Cacna1d	TGAAGGAGAAGATTGCGCCC	TTGCGGAATGAGTGGCTACG	190
Hcn1	CTCTTTTTGCTAACGCCGAT	CATTGAAATTGTCCACCGAA	291
Hcn2	CTTCACCAAGATCCTCAGTCTG	GGTCGTAGGTCATGTGGAAA	92
Hcn4	CCAGGAGAAGTATAAACAGGTGGAGCG	GTTGATGATCTCCTCTCGAAGTGGCTC	169
Col1a	GCGGACTCTGTTGCTGCTTGC	GACCTGCGGGACCCCTTTGT	125
Col3a	AGATCCGGGTCCTCCTGGCATTC	CTGGTCCCGGATAGCCACCCAT	194
Tgfb1	CGAGGTGACCTGGGCACCATCCATGAC	CTGCTCCACCTTGGGCTTGCGACCCAC	405
Mmp9	TCGCGTGGATAAGGAGTTCTC	ATGGCAGAAATAGGCTTTGTCTTG	82
Timp1	CAGATACCATGATGGCCCCC	CGCTGGTATAAGGTGGTCTCG	190
Timp2	CCAGAAGAAGAGCCTGAACCA	GTCCATCCAGAGGCACTCATC	112
Timp3	GGCCTCAATTACCGCTACCA	CTGATAGCCAGGGTACCCAAAA	135
Timp4	TGCAGAGGGAGAGCCTGAA	GGTACATGGCACTGCATAGCA	180
gapdh	CACCCTTCAAGTGGGCCCCG	CACCCTTCAAGTGGGCCCCG	227
Hprt1	GCAGGTCAGCAAAGAACTTATAGCC	CTCATGGACTGATTATGGACAGGAC	123